



HAL
open science

Evaluation of X-ray fluorescence for analysing critical elements in three electronic waste matrices: A comprehensive comparison of analytical techniques

Shaun T Lancaster, Eskil Sahlin, Marcus Oelze, Markus Ostermann, Jochen Vogl, Valérie Laperche, Solène Touze, Jean-Philippe Ghestem, Claire Dalencourt, Régine Gendre, et al.

► To cite this version:

Shaun T Lancaster, Eskil Sahlin, Marcus Oelze, Markus Ostermann, Jochen Vogl, et al.. Evaluation of X-ray fluorescence for analysing critical elements in three electronic waste matrices: A comprehensive comparison of analytical techniques. *Waste Management*, 2024, 190, pp.496 - 505. 10.1016/j.wasman.2024.10.015 . hal-04788656

HAL Id: hal-04788656

<https://brgm.hal.science/hal-04788656v1>

Submitted on 18 Nov 2024

HAL is a multi-disciplinary open access archive for the deposit and dissemination of scientific research documents, whether they are published or not. The documents may come from teaching and research institutions in France or abroad, or from public or private research centers.

L'archive ouverte pluridisciplinaire **HAL**, est destinée au dépôt et à la diffusion de documents scientifiques de niveau recherche, publiés ou non, émanant des établissements d'enseignement et de recherche français ou étrangers, des laboratoires publics ou privés.



Distributed under a Creative Commons Attribution 4.0 International License



Research Paper



Evaluation of X-ray fluorescence for analysing critical elements in three electronic waste matrices: A comprehensive comparison of analytical techniques

Shaun T. Lancaster^{a,*}, Eskil Sahlin^b, Marcus Oelze^c, Markus Ostermann^c, Jochen Vogl^c, Valérie Laperche^d, Solène Touze^d, Jean-Philippe Ghestem^d, Claire Dalencourt^e, Régine Gendre^e, Jessica Stammeier^f, Ole Klein^g, Daniel Pröfrock^g, Gala Košarac^h, Aida Jotanovic^h, Luigi Bergamaschiⁱ, Marco Di Luzioⁱ, Giancarlo D'Agostinoⁱ, Radojko Jaćimović^j, Melissa Eberhard^a, Laura Feiner^a, Simone Trimmel^a, Alessandra Rachetti^a, Timo Sara-Aho^k, Anita Roethke^l, Lena Michaliszyn^l, Axel Pramann^l, Olaf Rienitz^l, Johanna Irrgeher^a

^a Chair of General and Analytical Chemistry, Montanuniversität Leoben, Leoben, Austria

^b Research Institutes of Sweden (RISE), Borås, Sweden

^c Bundesanstalt für Materialforschung und -prüfung (BAM), Richard-Willstätter-Straße 11, 12489 Berlin, Germany

^d Bureau de Recherches Géologiques et Minières (BRGM), Water, Environment, Processes and Analysis Department, 3 Avenue Claude Guillemin, 45000 Orleans, France

^e ERAMET Ideas, 1 Rue Albert Einstein, 78190 Trappes, France

^f GFZ German Research Centre for Geosciences, Potsdam, Germany

^g Department for Inorganic Environmental Chemistry, Helmholtz-Zentrum Hereon, Max-Planck-Straße 1, 21502 Geesthacht, Germany

^h Institute of Metrology of Bosnia and Herzegovina, Branilaca Sarajeva 25, 71000 Sarajevo, Bosnia and Herzegovina

ⁱ Istituto Nazionale di Ricerca Metrologica (INRIM), Pavia, Italy

^j Jozef Stefan Institute (JSI), Ljubljana, Slovenia

^k Finnish Environment Institute (Syke), Research Infrastructure, Metrology, Mustialankatu 3, 00790 Helsinki, Finland

^l Physikalisch-Technische Bundesanstalt, Bundesallee 100, 38116 Braunschweig, Germany

ARTICLE INFO

Keywords:

XRF
WEEE
PCB
Battery
LED
Recycling

ABSTRACT

As the drive towards recycling electronic waste increases, demand for rapid and reliable analytical methodology to analyse the metal content of the waste is increasing, e.g. to assess the value of the waste and to decide the correct recycling routes. Here, we comprehensively assess the suitability of different x-ray fluorescence spectroscopy (XRF)-based techniques as rapid analytical tools for the determination of critical raw materials, such as Al, Ti, Mn, Fe, Co, Ni, Cu, Zn, Nb, Pd and Au, in three electronic waste matrices: printed circuit boards (PCB), light emitting diodes (LED), and lithium (Li)-ion batteries. As validated reference methods and materials to establish metrological traceability are lacking, several laboratories measured test samples of each matrix using XRF as well as other independent complementary techniques (instrumental neutron activation analysis (INAA), inductively coupled plasma mass spectrometry (ICP-MS) and ICP optical emission spectrometry (OES)) as an inter-laboratory comparison (ILC). Results highlighted key aspects of sample preparation, limits of detection, and

* Corresponding author.

E-mail addresses: shaun.lancaster@unileoben.ac.at (S.T. Lancaster), eskil.sahlin@ri.se (E. Sahlin), marcus.oelze@bam.de (M. Oelze), markus.ostermann@bam.de (M. Ostermann), jochen.vogl@bam.de (J. Vogl), v.laperche@brgm.fr (V. Laperche), s.touze@brgm.fr (S. Touze), jp.ghestim@brgm.fr (J.-P. Ghestem), claire.dalencourt@irsn.fr (C. Dalencourt), regine.gendre@eramet.com (R. Gendre), jessica.stammeier@gfz-potsdam.de (J. Stammeier), ole.klein@hereon.de (O. Klein), daniel.proefrock@hzg.de (D. Pröfrock), gala.kosarac@met.gov.ba (G. Košarac), aida.jotanovic@met.gov.ba (A. Jotanovic), l.bergamaschi@inrim.it (L. Bergamaschi), m.diluzio@inrim.it (M. Di Luzio), g.dagostino@inrim.it (G. D'Agostino), radojko.jacimovic@ijs.si (R. Jaćimović), melissa.eberhard@unileoben.ac.at (M. Eberhard), laura.feiner@stud.unileoben.ac.at (L. Feiner), simone.trimmel@unileoben.ac.at (S. Trimmel), alessandra.rachetti@unileoben.ac.at (A. Rachetti), timo.sara-aho@ymparisto.fi (T. Sara-Aho), anita.roethke@ptb.de (A. Roethke), lena.michaliszyn@ptb.de (L. Michaliszyn), axel.pramann@ptb.de (A. Pramann), olaf.rienitz@ptb.de (O. Rienitz), johanna.irrgeher@unileoben.ac.at (J. Irrgeher).

<https://doi.org/10.1016/j.wasman.2024.10.015>

Received 17 July 2024; Received in revised form 23 September 2024; Accepted 13 October 2024

Available online 19 October 2024

0956-053X/© 2024 The Author(s). Published by Elsevier Ltd. This is an open access article under the CC BY license (<http://creativecommons.org/licenses/by/4.0/>).

spectral interferences that affect the reliability of XRF, while additionally highlighting that XRF can provide more reliable data for certain elements compared to digestion-based approaches followed by ICP-MS analysis (e.g. group 4 and 5 metals). A clear distinction was observed in data processing methodologies for wavelength dispersive XRF, highlighting that considering the metals present as elements (rather than oxides) induces overestimations of the mass fractions when compared to other techniques. Eventually, the effect of sample particle size was studied and indicated that smaller particle size (<200 μm) is essential for reliable determinations.

1. Introduction

Critical raw materials, as defined by the European Commission (EC), are vital for the EU's economy and technological development, but face a high risk of supply disruptions (European Commission et al., 2017). Similar frameworks exist in other countries, including the USA (U.S. Department of Energy, 2023), China (Andersson, 2020), and Brazil (Ministry of Mines and Energy, 2021). Technology-critical elements (TCEs) is a name for a subset of these materials introduced by the European Cooperation in Science and Technology (COST) action TD1407 (Cobelo-García et al., 2015). Initially, the term included elements such as gallium (Ga), germanium (Ge), the platinum-group elements (PGEs) and the rare-earth elements (REEs), but it has been used to encompass various other elements since then (Klein et al., 2021; Qvarforth et al., 2022; Trimmel et al., 2023). In general, critical raw materials possess physicochemical properties essential for recent key applications in fields such as healthcare, transport, semiconductors and construction (Graedel et al., 2015; Gunn, 2014). Due to scarce domestic resources and low recycling rates, the EU relies heavily on imports, which prompted the European Critical Raw Materials Act released in 2023 to improve the stability of the supply chain. Hence, a particular focus is set on reducing dependency on non-EU sources for a subgroup of critical raw materials essential for energy, aerospace, defence and digitalisation, grouped under the term strategic raw materials (European Commission, 2023).

For many critical raw materials, recycling from waste electrical and electronic equipment (WEEE) is challenging due to the intricate design of electronic devices with a trend towards miniaturisation, along with the predominant use of hard-to-remove thermoset resins (Ayres et al., 2014; Mulcahy et al., 2022; Stuhlpfarrer et al., 2016, 2013). Additionally, the large variety in the design of electronic products further complicates recycling endeavours (Liu et al., 2023; Windisch-Kern et al., 2022). As decisions about the most effective recycling pathways require information about the economic value of the waste, the development of recycling strategies depends on sound analytical measurement procedures for the determination of recyclable critical raw material contents (Umbricht et al., 2022). Yet, the heterogeneity of waste streams, hard-to-digest sample matrices and low availability of standards and reference materials pose substantial analytical challenges (Bookhagen et al., 2018).

ICP-MS/ICP-OES/MP-AES: Inductively coupled plasma (ICP)-based methods have been utilized previously for the characterisation of e-waste materials, such as ICP – optical emission spectrometry (OES) (Andrade et al., 2019; Bookhagen et al., 2018), ICP – mass spectrometry (MS) (Bookhagen et al., 2018), and microwave plasma atomic emission spectrometry (MP-AES) (Gerold et al., 2024). These approaches typically allow for high throughput and robust analysis. ICP – tandem mass spectrometry (MS/MS) provides greater reliability through an additional mass filter that selects only one target mass-to-charge ratio (within 1 amu resolution) before minimizing spectral interferences using reaction gases, such as oxygen (Zhu et al., 2021), ammonia (Zhu et al., 2021), and nitrous oxide (Harouaka et al., 2021; Lancaster et al., 2023). Typically, these ICP-based techniques require the sample to be in an aqueous phase, which is where the limitations of this technique arise. Digestions of electronic waste material can be time consuming, challenging and can lead to biases if the solid material is inhomogeneous, the sample digestion is incomplete, or if the target analyte is lost due to

volatilization or precipitation.

INAA: Instrumental Neutron Activation Analysis (INAA) is an analytical technique based on activation of a stable isotope of the target analyte and gamma counting of the produced radioisotope. INAA can be applied in Rel-INAA or k_0 -INAA mode, where absolute nuclear data for particular nuclides were replaced by, so-called, k_0 -factors, which were experimentally determined and recommended to be used (Jaćimović et al., 2014). Besides panoramic analysis, one of the main advantages of this technique is the possibility to perform measurements of solid samples. Moreover, INAA is considered a primary method of measurement via a complete equation model linking the amount of substance to measured quantities that can be expressed in terms of SI units, as well as their uncertainties (D'Agostino and Di Luzio, 2024; Greenberg et al., 2011), which are suitable to be used as reference values for the characterization of materials. The need to use a neutron source makes the cost per analysis high and significantly limits the number of laboratories capable of applying this technique. Nevertheless, adoption of INAA is promising for the certification of WEEE reference materials and has already been used to quantify inorganic constituents in samples of printed circuit boards (Andrade et al., 2019).

XRF: Another more cost-effective method capable of solid sample analysis is x-ray fluorescence (XRF). The principle involves the use of x-rays to eject an electron from the inner shells of an atom, which in turn causes an electron from a higher shell to fall down to the inner shell and release a high-energy photon. Typically, wavelength dispersive (WD) or energy dispersive (ED) XRF instrumentation are used. WD-XRF spectrometers use a crystal to diffract, and thereby separate, the different wavelengths of x-rays emitted from by the sample, whereas ED-XRF spectrometers detect the different energies of x-rays emitted by the sample (Jenkins, 1999). Portable ED-XRF spectrometers (pXRF) have a resolution of 270 eV and a detection limit 10–20 times higher than non-portable ED-XRF devices, but can be used for on-site testing and have become a valuable tool for obtaining analytical results rapidly (Vanhoof et al., 2004; Verità et al., 1994). Total reflection X-ray fluorescence (TXRF) spectrometry is a multielement microanalytical technique also based on ED-XRF that is less commonly utilised, but is a growing area of research (Vanhoof et al., 2020). Here, a primary X-ray beam with a narrow energy range strikes a flat, polished (highly reflective) sample carrier at a very small angle so that total reflection occurs. This technique provides near elimination of the spectral background of the carrier and lower detection limits than conventional ED-XRF (Klockenkämper and von Bohlen, 2014).

While XRF-based techniques typically provide a simpler, more rapid analysis, challenges still remain. A lack of existing matrix-matched calibration standards, especially for electronic waste material, means that fully quantitative measurements of elemental components cannot be made. Semi-quantitative results can, however, be obtained as XRF instrumentation can be calibrated using a fundamental-parameter calibration. These results should be validated against existing quantitative methods and very little information currently exists about the performance of XRF for electronic waste samples. As such, this study aims to assess the suitability of XRF-based techniques for the quantification of critical and strategic raw materials, as well as TCEs, in three electronic waste matrices: printed circuit board (PCB), light emitting diode (LED), and Li-ion batteries. As certified reference materials for these matrices are scarce, this study provides an assessment of suitability through an

inter-laboratory comparison, with 11 institutions involved performing XRF-based analysis as well as complementary analysis with other techniques, such as ICP-MS/MS and INAA, to provide information on the performance of XRF for 39 elements, particularly focusing on Al, Ti, Mn, Fe, Co, Ni, Cu, Zn, Nb, Pd and Au.

2. Materials and methods

2.1. Samples

Four electronic waste materials were prepared and sent to participating laboratories for quantification of the metal mass fractions: one LED material, one Li-ion battery material, and two PCB materials of differing particle sizes (Fig. 1).

2.1.1. LED

A 17 kg batch of LEDs (Artemise, Vulaines, France) underwent shredding to achieve a particle size of approximately 10 mm using a shear shredder (Mecaroanne, Le Coteau, France). Subsequently, 7 kg was further shredded with a knife shredder (Fritsch GmbH, Germany) to achieve a size range of 2–4 mm. A sub-sample of 2 kg from the 7 kg batch (obtained with a riffle splitter) was shredded using an eccentric vibrating mill (Siebtechnik GmbH, Mülheim an der Ruhr, Germany), yielding a particle size of 200 μm for half of the sample. The remaining half (particle size between 200 μm and 2) underwent further processing using a SM 2000 cutting mill (Retsch GmbH, Haan, Germany) equipped with a sieve, reducing the particle size to less than 750 μm . The material was cooled with liquid nitrogen before milling and the process was repeated twice, with sieving in between to remove the < 200 μm fraction using an AS 200 control vibratory sieve shaker (Retsch GmbH). Subsequently, the material was processed in two stages (with constant cooling using liquid nitrogen) in a ZM 200 centrifugal mill (Retsch GmbH) at a rotation speed of approximately 233 s^{-1} , using a 500 μm sieve followed by a 200 μm sieve. The removable parts of the mill, including the sieve, rotor, and sample vessel, were also cooled with liquid nitrogen to prevent melting of the plastic components in the LED raw material. After each milling stage, the material was sieved to achieve a nominal particle

size of < 200 μm , with any remaining material milled again until no particles larger than 200 μm were left. All material with < 200 μm particle size were combined into one batch, of which sub-samples were sent to participating laboratories for analysis.

2.1.2. Li-ion battery

Li-ion battery black mass powder from non-compliant product dry pouch cells (contains no solvents) was shredded using a shear crusher RS30 (Untha, Kuchl, Austria) with a 15 mm control grid. A SM 200 cutting mill with stainless steel sieves (Retsch GmbH) was used to further reduce the sample size down to 500 μm . Finally, a cryogenic ball mill (Cryomill; Retsch GmbH) under liquid nitrogen allowed to reach the final required < 200 μm size.

2.1.3. PCB1 (<200 μm)

Approximately 500 kg of waste (Envie 2E Midi-Pyrénées, France) from the small WEEE category (audio and video appliances, toys, personal care products, culinary equipment, etc.) was obtained and dismantled manually to extract the PCB. The entire sample (485 kg) was first shredded with an industrial cutting mill (Bohmeier Maschinen GmbH, Germany) to a particle size < 30 mm. A quarter of the sample (122 kg obtained with a rotary divider for large samples, fed by a conveyor belt) was then shredded to a particle size < 10 mm and divided to obtain sub-sample masses of 4 kg. One of these subsamples was shredded to 750 μm using a cutting mill (SM 2000; Retsch GmbH) and subsequently milled to 200 μm in a universal grinder (FL1 Poittemille; Poittemille Company, Bethune, France) using ring holes. No particles were removed during the shredding steps. Sampling and processing methodologies are described in (Hubau et al., 2019; Touze et al., 2020).

2.1.4. PCB2 (2–4 mm)

Computer PCBs (from motherboards produced before 1994) were obtained (Valordis, Chalon-sur-Saône, France) and dismantled manually to extract the mother board PCBs. The whole sample (372 kg) was first shredded with a slow-rotating industrial shredder with stainless steel shears (Mecaroanne) to a particle size < 20 mm. This step was followed by primary sampling (described in detail in (Touzé et al., 2024)) to

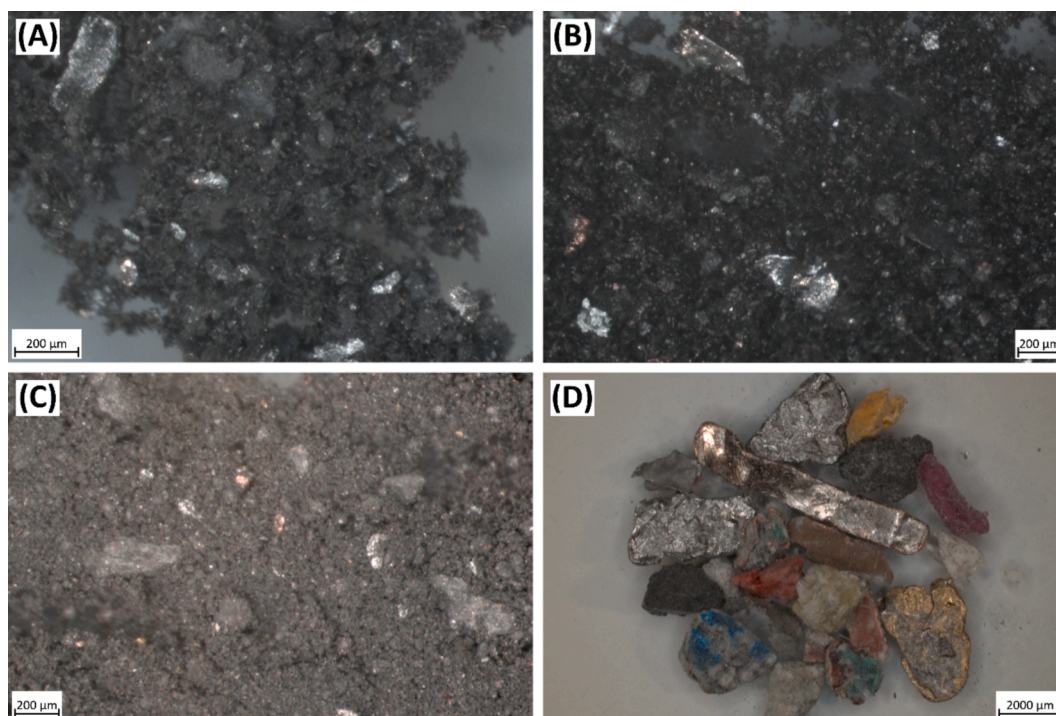


Fig. 1. Microscope images of (A) LED material, (B) Li-ion battery material, (C) PCB1 material (particle size < 200 μm , and (D) PCB2 material (particle size 2–4 mm).

produce 3 composite samples of approximately 30 kg, which were then shredded successively with 8 mm, 6 mm, 4 mm and 2 mm sieves in a lab knife mill with tungsten carbide knives (Pulverisette 19; Fritsch). The samples were then divided by riffle splitters (chute widths of 60 mm and 30 mm) to obtain 3 samples of 2.6 kg each. One of these sample batches was used for the study on the influence of particle size on the measurements.

2.2. Analysis

The PCB1, LED, and Li-battery materials with particle sizes < 200 µm were sent to partner laboratories for elemental analysis. Table 1 provides a summary of the analytical methods used for each data set submitted. One key distinction arose with WD-XRF, whereby laboratories opted to quantify the metal contents either assuming the target analytes to be in elemental form, or assuming them to be present as oxides and subsequently calculating back to the elemental content stoichiometrically. Additionally, certain laboratories opted to perform a calcination step by heating the sample at 550 °C for 6 h in order to remove part of the organic matrix (mass loss on calcination (550 °C): LED = (26.1 ± 0.3)%; Li-ion battery = (19.2 ± 0.9)%; PCB1 = (17.2 ± 0.2)%; PCB2 = (19.6 ± 4.3)% prior to sample digestions or analysis.

2.3. Data treatment – The Horwitz function

The Horwitz function was used in this study to assist in the inter-

pretation of the results from the inter-laboratory comparison. Originally, the function was derived for the evaluation of methods for food and drug analysis (Horwitz, 1982), but it has since been applied to many proficiency tests of different sample matrices (Horwitz and Albert, 2006; Thompson, 2004), such as geological samples in the GeoPT programme (Meisel et al., 2022). The function describes the expected between-laboratory coefficient of variation (CV) as follows:

$$CV (\text{in } \%) = 2^{(1-0.5 \cdot \log w_{\text{mode}})}$$

where w_{mode} in this study represents the statistically determined mode (most frequent value) of the mass fractions (mass of the analyte divided by the total mass of sample) obtained between-laboratory data. For interpretation of the data, two intervals have been provided: single CV (68 % confidence interval) and two-times CV (95 % confidence interval). The advantage of this approach is that the expected CV does not depend on the between-laboratory variation, only on the mode.

3. Results and discussion

3.1. Trends observed from the inter-laboratory comparison

In the following section, only selected figures from the inter-laboratory comparison are shown in order to discuss notable trends and observations. The full set of figures from each element determined in the e-waste materials are provided as an interactive PDF document in

Table 1

Summary of analytical methods used by participating laboratories in the inter-laboratory comparison (ILC) study. The results have been anonymized by using a lab code. Some laboratories have provided more than one analysis by different techniques, each with a different lab code. An extended description of each analytical method used by each participating laboratory has been provided in supplementary information A.

Lab Code	Technique	Calcination of sample	Sample preparation	Evaluation method	Additional notes
L1	pXRF	No	Pressed pellet (no binding agent)	Factory calibration (mining)	
L2	pXRF	No	Powder	Factory calibration (mining)	
L3	pXRF	No	Powder	Factory calibration (mining)	
L4	pXRF	No	Powder	Factory calibration (mining)	
L5	pXRF	No	Pressed pellet (no binding agent)	Factory calibration (mining)	
L6	pXRF	Yes	Pressed pellet (10 % wax binder)	Factory calibration (mining)	
L7	pXRF	Yes	Powder	Factory calibration (mining)	
L8	pXRF	Yes	Pressed pellet (14 % wax binder)	Factory calibration (mining)	
L9	WD-XRF	No	Pressed pellet (10 % wax binder)	Fundamental parameter	Measured as elements
L10	WD-XRF	No	Powder	Fundamental parameter	Measured as elements
L11	WD-XRF	Yes	Pressed pellet (10 % wax binder)	Fundamental parameter	Measured as elements
L12	WD-XRF	Yes	Powder	Fundamental parameter	Measured as oxides
L13	WD-XRF	Yes	Pressed pellet (10 % wax binder)	Fundamental parameter	Measured as oxides
L14	WD-XRF	Yes	Pressed pellet (10 % wax binder)	Fundamental parameter	Measured as oxides
L15	WD-XRF	Yes	Pressed pellet (14 % wax binder) + back filler	Fundamental parameter	Measured as oxides
L16	TXRF	No	Pressurized aqua regia	Fundamental parameter	
L17	TXRF	No	Pressurized aqua regia including particle suspension	Fundamental parameter	
L18	TXRF	No	Aqueous particle suspension	Fundamental parameter	
L19	ICP-MS/ MS	No	Aqua regia	External calibration	
L20	ICP-MS/ MS	Yes	Peroxide fusion	External calibration	
L21	ICP-MS/ MS	Yes	Aqua regia/HBF ₄	External calibration	
L22	ICP-MS/ MS	Yes	Aqua regia/H ₂ O ₂	External calibration	
L23	ICP-MS/ MS	Yes	HF/HCl/HNO ₃	External calibration	
L24	ICP-MS/ MS	No	HF/HCl/HNO ₃	External calibration	
L25	ICP-MS/ MS	No	Pressurized aqua regia digestion	External calibration	
L26	ICP-MS/ MS	No	Inverse aqua regia/HBF ₄	External calibration	
L27	HR-ICP-MS	Yes	HNO ₃ /HBF ₄ /H ₂ O ₂	Standard addition	
L28	ICP-OES	No	HF/HCl/HNO ₃	External calibration	
L29	INAA	No	Powder in a polyethylene container	k ₀ -INAA standardization	Non-destructive technique
L30	INAA	No	Pressed pellet (no binding agent)	Rel-INAA and k ₀ -INAA standardization	Non-destructive technique

supplementary information B. Good agreement with the Horwitz function typically relies on participating laboratories using validated methods, including both sample preparation and analysis. Here, the function is still a good indicator for measurement quality, despite non-validated methods for the presented e-waste matrices being used. In general, it can be seen that while there are good agreements between the different techniques for certain major elements, such as Cu, Co or Mn (Supplementary B), in most cases, the between-laboratory variability exceeds that expected from the Horwitz function and no concrete explanation regarding sample preparation or analysis effects exists. This indicates an inherent inhomogeneity of the test samples, which is likely as the matrix contains “large” particles of the metal analytes ($<200\ \mu\text{m}$), as shown in microscope images of the samples in Fig. 1A–C. Such inhomogeneity is not accounted for within the Horwitz function, however it still provides a useful guide here to identify measurement issues for the more extreme outliers.

3.1.1. Sample preparation for pXRF and WD-XRF

For the critical raw materials that are present in high quantities ($>10\ 000\ \text{mg kg}^{-1}$), such as Ti (in PCB1), Co (in Li-ion battery) Fe, Cu, and Zn (Supplementary B), pXRF generally provided results in-line with that of the comparative techniques, regardless of the sample preparation used. For WD-XRF, however, it became apparent that sample preparation, as well as the applied software calculations, plays a crucial role in the accurate quantification of metals in e-waste. Light element components ($Z < 10$) cannot be directly determined by XRF, as the characteristic wavelengths emitted by these elements are reabsorbed by the sample. Contrary to the pXRF systems, which seem to reasonably estimate the balance of these light-element components in the e-waste matrix (such as carbon, oxygen, and lithium), WD-XRF does not seem to account for these elements particularly well. As such, this leads to an over-determination of the analyte mass fractions when calculating the mass fractions in element mode (referred to in the figures as WD-XRF (E)), which has been observed here for many elements, such as Al, Ti, Cr, Mn, Co, Cu, Zn (in PCB1), and Nb (Supplementary B). However, applying a calcination step to remove part of the matrix and convert some metals to oxides (depending on the temperature) generally allows for more reliable results for these aforementioned elements, as long as the calculation of the mass fraction by the software is performed for oxides (referred to in the figures as WD-XRF (O)) and subsequently converted back to elemental mass fractions stoichiometrically. Conversely, the opposite was observed for Zn (in LED) and Ni (Supplementary B), where the oxide approach for these elements

underdetermined their mass fractions. WD-XRF software does allow users to specify which elements to determine as oxides or elements, and the data provided here is helpful for assisting in deciding how to process the data for each analyte for each e-waste matrix.

While most participants opted to prepare pressed pellets for WD-XRF, it may also be possible to analyse powders directly depending on the instrumentation. However, obtained results from powders also indicate the same trend regarding calcination and the determination of metals as oxides described previously (Supplementary B; L10 and L12). Another traditional sample preparation method is the production of fused bead (Dhara et al., 2020; Younis et al., 2017), which provides a much more homogeneous distribution of the metals that can be measured as elements. However, one participating laboratory reported that the high metal content of the e-waste material caused issues with the sample preparation, with the metals fusing with (and destroying) a Zr crucible, which in turn caused the Zr to leach into the glass bead. Therefore, the glass bead sample preparation method is likely not recommendable for these matrices.

3.1.2. Analysis of minor components by pXRF and WD-XRF

The mass fractions of TCEs were found to be very low for all materials (typically $< 100\ \text{mg kg}^{-1}$), with the exception of Co in the Li-ion battery material where it is present as a major component ($w_{\text{mode}}(\text{Co}) = 6.4\ \%$). In most cases, XRF data for the TCEs were not provided as they were below the detection limits of this technique. Au is a precious metal that contributes significantly to the economic value of waste. XRF results for Au were provided for PCB1 and LED materials, but only by pXRF (Fig. 2). This could be due to the software of WD-XRF, which generally implements a user-defined cut-off value whereby results obtained under a certain mass fraction are removed from the report. Results for Au show a very large positive bias for the results using pXRF, which is likely due to the mass fraction of Au in the samples (PCB1: $w_{\text{mode}}(\text{Au}) = 38\ \text{mg kg}^{-1}$; LED: $w_{\text{mode}}(\text{Au}) = 5.4\ \text{mg kg}^{-1}$) being below the detection limits of pXRF, as well as the possibility of large interferences from percentage-levels of Zn and Br, whose signals overlap with that of Au ($L\alpha$ and $L\beta$ respectively). Here, interferences are too large to be handled, leading to unreliable results. It should be noted, however, that previous studies have shown pXRF to be effective in the determination of Au in e-waste samples containing higher Au contents, such as mobile phone PCBs (Ippolito et al., 2021).

Similar observations were made for Pd in the PCB1 material, where the results provided by pXRF were closer to the comparative data from ICP-MS/MS ($w_{\text{mode}}(\text{Pd}) = 14\ \text{mg kg}^{-1}$). However, several replicate

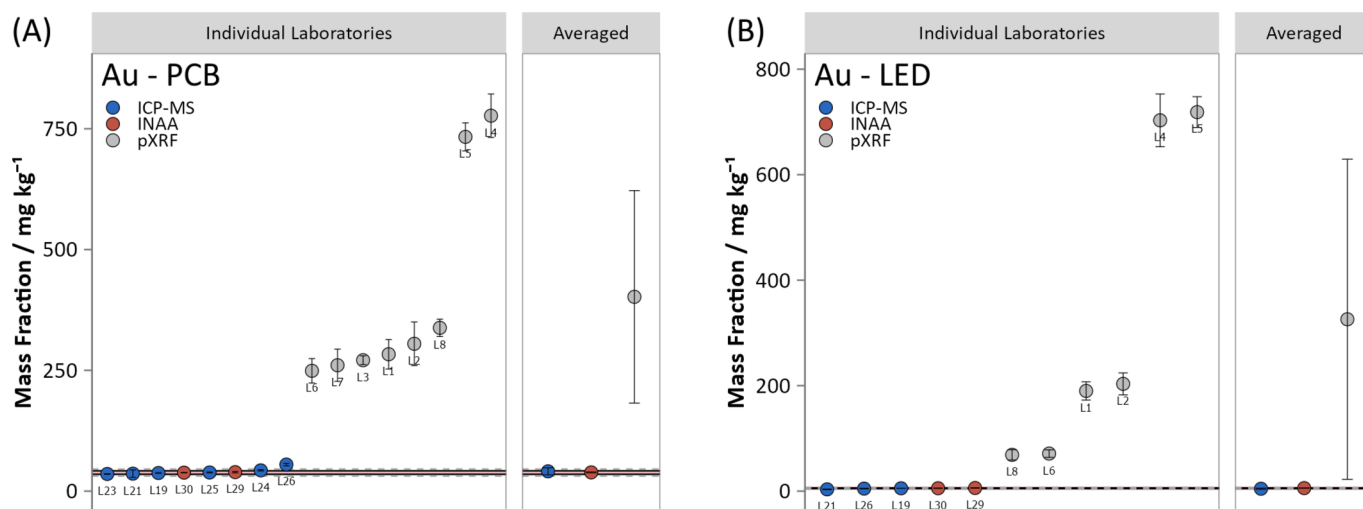


Fig. 2. Inter-laboratory comparison results for the mass fraction of Au in (A) PCB1 matrix and (B) LED matrix. The pink line represents the statistical mode, the black line and grey dotted line represent 1 SD and 2 SD of the Horwitz function. Error bars denote a single standard deviation, with the exception of the INAA results which denote the standard uncertainty ($k = 1$). (For interpretation of the references to colour in this figure legend, the reader is referred to the web version of this article.)

determinations were reported as below the detection limit by the software and were not included in the final value, hence the presented results given by pXRF cannot be considered reliable.

While Co could be successfully determined by pXRF in Li-ion batteries, the technique displayed a consistent underestimation of Co in PCB material (Supplementary B), which had a much lower content ($w_{\text{mode}}(\text{Co}) = 757 \text{ mg kg}^{-1}$). This may also be a result of the high detection limits coupled with over correction of spectral interferences from the presence of high levels of Fe (discussed further in section 3.2.). In contrast, Co mass fractions determined by WD-XRF (calculated as oxides) were in good agreement with the INAA and ICP-MS/MS results, though with high between-laboratory variation. It is clear that lower levels of the target analyte have a large impact on the reliability of the pXRF technique compared to WD-XRF. From this study, pXRF would be recommended for analytes with a mass fraction greater than 1000 mg/kg.

3.1.3. TXRF

The TXRF technique allows for fine powders and pulverized solid samples to be prepared as liquid suspensions, of which a few microliters are pipetted on the sample carrier and dried as a thin film, as well as the analysis of aqueous sample digests if particle suspensions are not possible. Although minimal data has been provided for TXRF in this study, it can be seen that the use of a pressurized aqua regia digestion followed by analysis provided results in line with the other comparative techniques. For Li-ion battery material, TXRF data acquired by aqueous suspension was additionally provided. It was observed that analysis performed using an aqueous suspension of only the solid material consistently gave a very low precision, while the mean value itself showed an under-determination of the analyte mass fractions compared to other techniques. As the average particle size of the samples was approximately 200 μm , the materials were likely too coarse for the preparation of aqueous suspensions. This was experimentally verified as a representative 10 μl aliquot of an aqueous suspension of any of the sample types was impossible to pipette due to rapidly descending large sample particles. The particles in these samples have inhomogeneous surfaces (Fig. 1), which influences the total reflection of the beam. Previous literature regarding the direct measurement of solid samples by TXRF ideally requires particle sizes of < 10 μm , with an average particle size of 1 μm (Fernández-Ruiz et al., 2018; Klockenkämper and von Bohlen, 1989), which is far smaller than the particle size fraction used in this study and, given the difficulty and time consuming nature of milling electronic waste samples, may not be practical for these samples. Additionally, the particles must be chemically homogeneous (Fernández-Ruiz and García-Heras, 2007), which is not the case for the electronic waste matrices used in this study (Fig. 1). For these reasons, it should be recommended to perform measurements of digested electronic waste samples using TXRF.

3.1.4. Sample preparation for ICP-based methods

Several different digestion methods were used for solubilisation prior to analysis with ICP-based methods. Primarily, variations of aqua regia were used, with additions of H_2O_2 , HBF_4 , or HF as modifiers. Results for the major components reveal good comparison of results for Cr, Mn, Fe, Co, Ni, Cu, and Zn, as well as for the minor components Pd and Au (Supplementary B). This implies that the use of aqua regia would be enough to quantitatively extract these particular metals. Results from calcination of the samples did not appear to show a distinct difference to non-calcinated samples, however it should be noted that laboratories that did not perform a calcination step typically used harsher digestion conditions (e.g. high pressure, HF).

Although the group 4 and 5 transition metals Ti, Zr, and Nb showed good agreement between XRF and INAA data, severe biases were observed in the ICP-MS/MS and ICP-OES determinations (Supplementary B). In this case, sample preparation plays a key role as hydrofluoric acid is required in order to quantitatively solubilize these

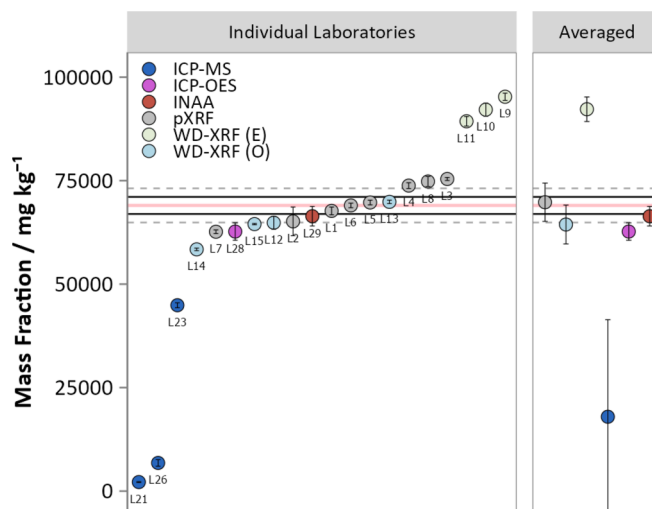


Fig. 3. Inter-laboratory comparison results for the mass fraction of Ti in PCB1 matrix. The pink line represents the statistical mode, the black line and grey dotted line represent 1 SD and 2 SD of the Horwitz function. For WD-XRF, (E) indicates the metals were assumed to be present as elements and (O) indicates the metals were assumed to be present as oxides (and converted back to elemental mass fraction). Error bars denote a single standard deviation, with the exception of the INAA results which denote the standard uncertainty ($k = 1$). (For interpretation of the references to colour in this figure legend, the reader is referred to the web version of this article.)

particular elements and stabilize them in solution (i.e. by preventing hydrolysis). In this case, both the WD-XRF (determined as oxides) and pXRF methodology appear to provide more reliable results (comparable to INAA) than ICP-based methods, especially for Ti in the PCB1 sample (Fig. 3), which is present as a major component ($w_{\text{mode}}(\text{Ti}) = 6.9\%$).

3.1.5. Determination of the light elements

The previous observation for typical determinations using acid digestion, as well as the aforementioned detection limit issues of the

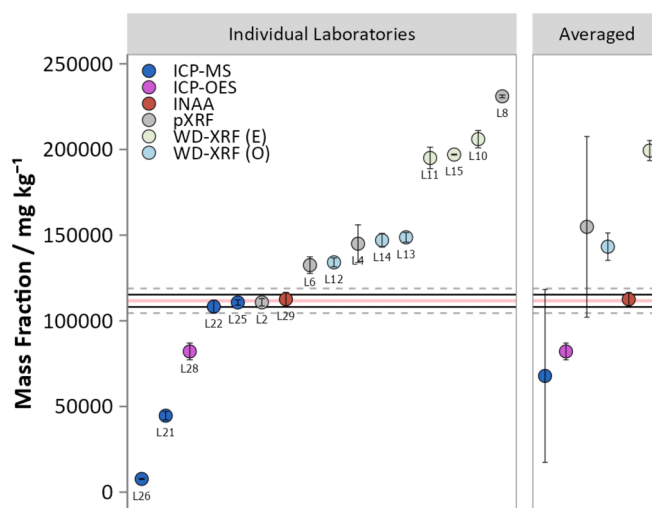


Fig. 4. Inter-laboratory comparison results for the mass fraction of Al in Li-ion battery matrix. The pink line represents the statistical mode, the black line and grey dotted line represent 1 SD and 2 SD of the Horwitz function. For WD-XRF, (E) indicates the metals were assumed to be present as elements and (O) indicates the metals were assumed to be present as oxides (and converted back to elemental mass fraction). Error bars denote a single standard deviation, with the exception of the INAA results which denote the standard uncertainty ($k = 1$). (For interpretation of the references to colour in this figure legend, the reader is referred to the web version of this article.)

XRF-based techniques, can also be noted for the determination of Al, as seen for Li-ion batteries in Fig. 4.

Al is a light element and difficult to determine by XRF-based techniques as the photons emitted by light elements are easily absorbed by the air between the sample and the detector, leading to very high detection limits. Because of this, the results from pXRF and WD-XRF do not compare well with INAA. Results obtained using WD-XRF show low between-laboratory variation for measurements conducted under similar conditions (assuming oxides or elements), with results generated by assuming the metals are present as oxides showing closer agreement with the INAA results – though still with a significant bias due to the detection limits. This is in contrast to the pXRF results, where the variability between laboratories is much higher, as the detection limits are much higher for pXRF because there is no option to measure the sample under an inert atmosphere (e.g. helium) to mitigate the reduction in sensitivity from the presence of air, unlike with WD-XRF. Additionally, for pXRF, the use of a polypropylene film between the instrument and the sample (facilitating analyses directly on the powder sample) appears to influence the determination of light elements. Results provided for both Al and Si in pelletized samples that did not use the film (L1 and L8) generally provided higher results than the powder samples or pressed pellets measured using a film (Supplementary B). For these reasons, XRF cannot be recommended for determinations of Al in electronic waste matrices presently. A possible resolution would be to use matrix-matched calibration standards to create a custom WD-XRF calibration that would improve the biases observed. However, several calibration standards are required for this process and such certified standards do not currently exist.

ICP-MS/MS and ICP-OES data produced using HF- or HBF₄-based digestions typically showed under-determinations of the Al mass fraction, whereas digestions without these reagents yielded results comparable to INAA. This may be due to the common-ion effect, where AlF₃ has a much lower solubility product than AlCl₃ (Lide, 2004) and may precipitate due to the high concentration of available fluoride ions in addition to the high Al content of the sample ($w_{\text{mode}}(\text{Al}) = 11\%$). These observations were replicated in the LED material ($w_{\text{mode}}(\text{Al}) = 28\%$), however, for the PCB1 material, only two of the four fluorine-based acid digestions displayed large under-determinations. This could be due to the lower mass fraction of Al in the PCB1 sample ($w_{\text{mode}}(\text{Al}) = 4.6\%$). This study highlights that consideration and understanding of biases contributing to measurement uncertainties is important in order to avoid reporting of unreliable results.

3.2. Comparison of WD-XRF and pXRF

The inter-laboratory comparison highlighted differences in results obtained between pXRF and WD-XRF. This was especially true for elements present in quantities less than 1000 mg kg⁻¹, such as Co (in PCB1) and Mo (Supplementary B), where pXRF underestimated the mass fractions, as well as the aforementioned overestimations of Au (Fig. 2) and Pd. The detection limits and x-ray peak resolution (FWHM) are generally not as good with pXRF compared to WD-XRF. A comparison of the resolution in different parts of the wavelength range is shown in Fig. 5 (pXRF spectra obtained with Niton XL3t GOLDD+ (Thermo Scientific) and WD-XRF spectra obtained with ARL AdvantX Sequential XRF IntelliPower (Thermo Scientific)).

In the upper part of the spectrum (e.g. 20 keV), the resolution of the two techniques are approximately the same (Fig. 5A). However, at lower energies, the resolution of the pXRF becomes poor compared to WD-XRF (Fig. 5B and 5C). No change to the resolution was observed for pXRF when swapping between the spectra obtained using the different energy filters. Two relevant examples of analyte peaks are shown in Fig. 5D and 5E. In Fig. 5D, the AuL α peak in the PCB1 sample ($w_{\text{mode}}(\text{Au}) = 38\text{ mg/kg}$) is marked showing that it is located at the tail of a WL β peak using WD-XRF. With pXRF, the AuL α peak is overlapped to a much larger extent by a broad peak mainly from ZnK β and WL β . In Fig. 5E, the CoK α

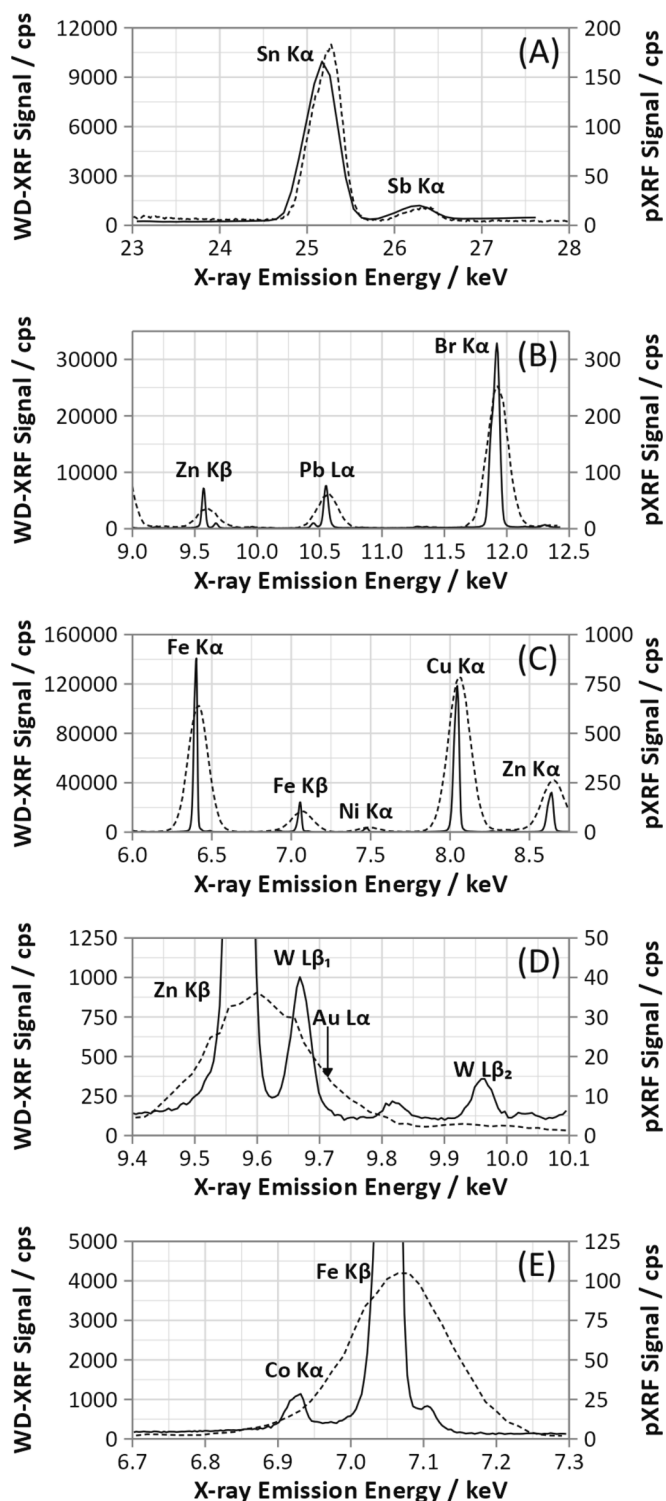


Fig. 5. Comparison of WD-XRF (solid line) and pXRF (dashed line) for the PCB1 sample with particle size of < 200 μm . (A), (B) and (C) depicts spectra from different parts of the useful wavelength range showing peaks for main components. (D) shows an enlarged spectrum where the position of the AuL α peak is marked and (E) enlarged spectrum where the position of the CoK α peak is marked.

peak in the PCB1 sample ($w_{\text{mode}}(\text{Co}) = 760\text{ mg/kg}$) is marked showing a well-defined peak with only minor overlap using WD-XRF. Using pXRF, the CoK α peak has a major overlap from FeK β . Clearly, corrections due to spectral overlap are much larger for pXRF than for WD-XRF,

indicating the possibilities to determine trace levels of components, such as the TCEs, with pXRF are poor.

3.3. Effect of particle size

In order to observe the effect of the sample particle size on the measurement quality, selected laboratories were provided a sub-sample of a batch of PCB2 material with a particle size of 2–4 mm (Fig. 1D). The PCB material was specifically selected for this work as the ILC highlighted that it contains the widest variety of elements that could be studied. Figures for each element where results were provided by partners can be found in Supplementary B. In general, the between-laboratory variation was very high due to the extent of inhomogeneity of the test sample, but the within-laboratory variations showed a mixture of very high and very low variability (e.g. Cu and Zn; Supplementary B). It should be noted, though, that XRF typically provided excellent precision on repeated measurement of single preparations, indicating that the difference in particle size did not affect the overall instrument precision.

In order to provide further context to the effect of particle size on replicate precision, pXRF was used to generate 100 replicate measurements of PCB materials with 2–4 mm and < 200 μm by shaking the sample between each measurement. From these 100 real observations, the mass fractions provided by pXRF were rearranged and averaged sequentially 1000 times (using the statistical program R (R Core Team, 2024)) to simulate the expected relative standard deviation (s_r , denoted hereinafter as RSD) of replicate measurements between the two particle sizes. The resulting plots for each element are provided in Supplementary B, however the plots for Cu and Zn have been isolated for discussion and are provided in Fig. 6.

As expected, the achievable replicate precision for the test sample with a lower particle size is far lower than that of the larger particle size, which has been observed previously (Hubau and Moreau, 2022). However, this study also demonstrates the general improvement of measurement quality with the number of replicate determinations made based on simulations using real generated results. At low numbers of replicate determinations (e.g. $n = 3$), there is a very wide variability in the expected precision. For example, for Cu in the 2–4 mm fraction, the RSDs obtained ranged from 1.7 % to 83 % (Fig. 6A). As more replicate determinations are made, the possible precision that could be obtained converges towards the population mean with less variation – in the case of Cu in the 2–4 mm fraction, the RSD obtained for 100 measurements was 28 %. The same variation is also observed with the simulated mean values, which potentially indicates why such high variation exists for the mean mass fractions determined in the inter-laboratory comparison of

the 2–4 mm particle size test sample, yet the precision for some determinations may be low (Supplementary B). For all of the elements determined in the < 200 μm fraction with ED-XRF, these trends were also observed, however the precision obtained was much greater. It was even possible to obtain less than 10 % RSD for all major elements when measuring 10 or more replicates, thus highlighting the importance of replicate determinations when analysing samples. In both cases, the mean RSD (Fig. 6A; black line) shows an initial increase before quickly reaching an asymptote at the population mean RSD. This is expected to be due to biases in statistics using low degrees of freedom, which leads to an underestimation of the standard deviation.

A second observation comes when extreme statistical outliers are included in the determination of the mean and standard deviation. These can only be considered statistical outliers as, in reality, the results generated are due to real-world effects, such as a large particle of a single-element metal reaching the bottom of the container and is therefore closer to the XRF detector. Here, the effect of these statistical outliers can be seen in Fig. 6B, where the simulated RSDs for Zn in the 2–4 mm fraction, which contained 7 statistical outliers (Grubb's test), form distinct bands across a wide range of RSD values depending on the number of statistical outliers measured. The observed increase in mean RSD obtained (Fig. 6B; black line) indicates that increasing the number of replicates means that the probability of the inclusion of such statistical outliers become more likely than not. Such observations may also be extrapolated to other analytical techniques, such as ICP-MS, due to the error involved in sampling the material. While it is clear that measurement quality can be improved by performing more replicate measurements as it compensates for heterogeneity, the data indicates that, for elements where extreme statistical outliers may be expected, it is not trivial to suggest a number of replicates that strikes a balance between reliability and reasonability.

4. Conclusions

This study highlights the importance of measurement quality and understanding sources of bias during measurements. Generally, it can be seen that, for WD-XRF, combustion of the materials followed by quantification of the metal oxides provides overall more reliable results in the analysis of e-waste, whereas for pXRF, the results were generally similar independent of the sample preparation. While XRF was generally found to provide reliable results comparable to other reference techniques for the major elements, limitations still exist with the determination of minor components, especially the TCEs. Improvements may be possible in future if matrix-specific calibration standards could be made to reduce biases, as well as developments in instrumentation to push past the

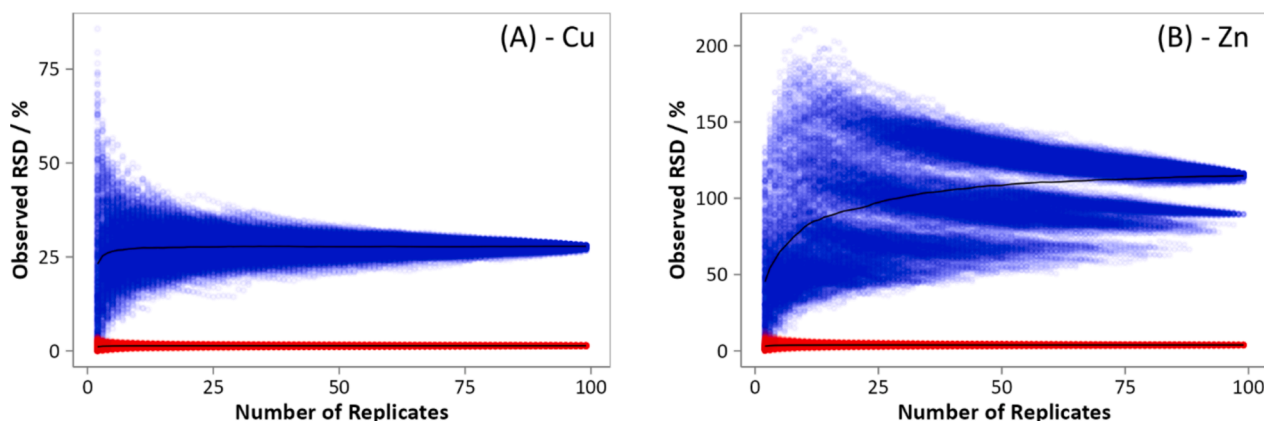


Fig. 6. Distribution of simulated RSDs with number of replicate determinations for Cu (A) and Zn (B) in PCB material with a particle size of 2–4 mm (blue) and < 200 μm (red) using pXRF. 100 replicate measurements were made. Using this data set, a simulation of the distribution of RSDs expected for each element was generated by rearranging and averaging the data sequentially, and repeating this process 1000 times. The black line indicates the average RSD for a given number of replicate determinations. (For interpretation of the references to colour in this figure legend, the reader is referred to the web version of this article.)

current detection limits. Importantly, the data also highlights that ICP-MS methodology used widely in the field of routine analysis is itself also not without error, as sample preparation plays a crucial role in its ability to provide reliable results. The study underscores the importance of reliable methods for the determination of critical raw materials and critical metals, as accurate measurements are essential for advancing both scientific understanding and practical applications in resource recovery and sustainability in recycling industries. As decisions about the most effective recycling pathways require information about the economic value of the waste, the development of recycling strategies depends heavily on reliable analytical methods to quantify the presence of critical raw materials accurately. Ensuring the reliability of these methods is essential for addressing circular economy initiatives by the European Commission and achieving the Sustainable Development Goals (SDGs). The accurate determination of raw materials in e-waste is crucial for effective waste management, as it enables precise identification and recovery of valuable materials, thereby enhancing recycling efficiency and reducing environmental impact. Ultimately, this contributes to a more sustainable future by promoting resource conservation and minimizing the ecological footprint of electronic waste.

CRedit authorship contribution statement

Shaun T. Lancaster: Writing – review & editing, Writing – original draft, Visualization, Investigation, Data curation, Conceptualization. **Eskil Sahlin:** Writing – review & editing, Writing – original draft, Validation, Investigation. **Marcus Oelze:** Validation, Investigation. **Markus Ostermann:** Validation, Investigation. **Jochen Vogl:** Supervision, Resources. **Valérie Laperche:** Validation, Investigation. **Solène Touze:** Validation, Investigation. **Jean-Philippe Ghestem:** Writing – review & editing, Supervision, Resources. **Claire Dalencourt:** Resources. **Régine Gendre:** Supervision, Resources. **Jessica Stammeier:** Validation, Investigation. **Ole Klein:** Writing – review & editing, Validation, Investigation. **Daniel Pröfrock:** Writing – review & editing, Validation, Supervision, Resources, Investigation. **Gala Košarac:** Validation, Investigation. **Aida Jotanovic:** Validation, Supervision, Resources, Investigation. **Luigi Bergamaschi:** Validation, Investigation. **Marco Di Luzio:** Writing – review & editing, Validation, Investigation. **Giancarlo D'Agostino:** Writing – review & editing, Supervision, Resources. **Radojko Jaćimović:** Writing – review & editing, Validation, Investigation. **Melissa Eberhard:** Validation, Investigation. **Laura Feiner:** Validation, Investigation. **Simone Trimmel:** Writing – review & editing, Validation, Investigation. **Alessandra Rachetti:** Writing – review & editing, Validation, Investigation. **Timo Sara-Aho:** Writing – review & editing, Validation, Investigation. **Anita Roethke:** Validation, Investigation. **Lena Michaliszyn:** Validation, Investigation. **Axel Prammann:** Validation, Investigation. **Olaf Rienitz:** Validation, Supervision, Resources, Investigation. **Johanna Irrgeher:** Writing – review & editing, Supervision, Resources, Project administration, Funding acquisition, Conceptualization.

Declaration of competing interest

The authors declare that they have no known competing financial interests or personal relationships that could have appeared to influence the work reported in this paper.

Acknowledgements

This project (20IND01 MetroCycleEU) has received funding from the EMPIR programme co-financed by the Participating States and from the European Union's Horizon 2020 research and innovation programme. The authors would like to thank Thomas C. Meisel for fruitful discussions and providing existing R code to help process the data.

Appendix A. Supplementary data

Supplementary data to this article can be found online at <https://doi.org/10.1016/j.wasman.2024.10.015>.

Data availability

Data will be made available on request.

References

- Andersson, P., 2020. Chinese assessments of “critical” and “strategic” raw materials: Concepts, categories, policies, and implications. *Extr. Ind. Soc.* 7, 127–137. <https://doi.org/10.1016/j.exis.2020.01.008>.
- Andrade, D.F., Machado, R.C., Bacchi, M.A., Pereira-Filho, E.R., 2019. Proposition of electronic waste as a reference material-part 1: Sample preparation, characterization and chemometric evaluation. *J. Anal. At. Spectrom.* 34, 2394–2401. <https://doi.org/10.1039/c9ja00283a>.
- Ayres, R.U., Méndez, G.V., Peiró, L.T., 2014. Recycling Rare Metals. In: Worrell, E., Reuter, M.A. (Eds.), *Handbook of Recycling: State-of-the-Art for Practitioners, Analysts, and Scientists*. Elsevier, Waltham, MA.
- Bookhagen, B., Obermaier, W., Oppen, C., Koeberl, C., Hofmann, T., Prohaska, T., Irrgeher, J., 2018. Development of a versatile analytical protocol for the comprehensive determination of the elemental composition of smartphone compartments on the example of printed circuit boards. *Anal. Methods* 10, 3864–3871. <https://doi.org/10.1039/c8ay01192c>.
- Cobelo-García, A., Filella, M., Croot, P., Frazzoli, C., Du Laing, G., Ospina-Alvarez, N., Rauch, S., Salaun, P., Schäfer, J., Zimmermann, S., 2015. COST action TD1407: network on technology-critical elements (NOTICE)—from environmental processes to human health threats. *Environ. Sci. Pollut. Res.* 22, 15188–15194. <https://doi.org/10.1007/s11356-015-5221-0>.
- D'Agostino, G., Di Luzio, M., 2024. Development and application of a comprehensive measurement equation for the direct comparator standardization method of Instrumental Neutron Activation Analysis. *Spectrochim. Acta - Part B At. Spectrosc.* 218, 106997. <https://doi.org/10.1016/j.sab.2024.106997>.
- Dhara, S., Sanyal, K., Misra, N.L., 2020. Universal EDXRF method for multi-elemental determinations using fused bead specimens. *Anal. Sci.* 36, 113–119. <https://doi.org/10.2116/analsci.19P196>.
- European Commission, Directorate-General for Internal Market, Industry, Entrepreneurship and SMEs, Pennington, D., Tzimas, E., Baranzelli, C., Van Maercke, A., Dewulf, J., Manfredi, S., Nuss, P., Grohol, M., Kayam, Y., Solar, S., Vidal-Legaz, B., Talens Peiró, L., Mancini, L., Ciupagea, C., Godlewska, L., Dias, P., Pavel, C., Blagoeva, D., Blengini, G., Nita, V., Latunussa, C., Torres De Matos, C., Mathieux, F., Marmier, A., 2017. Methodology for establishing the EU list of critical raw materials – Guidelines. Publications Office. doi: 10.2873/769526.
- European Commission, 2023. 'Proposal for a regulation of the European Parliament and of the Council establishing a framework for ensuring a secure and sustainable supply of critical raw materials and amending Regulations (EU) 168/2013, (EU) 2018/858, 2018/1724 and (EU) 2019/1020.' COM (2023) 160 final.
- Fernández-Ruiz, R., García-Heras, M., 2007. Study of archaeological ceramics by total-reflection X-ray fluorescence spectrometry: Semi-quantitative approach. *Spectrochim. Acta - Part B At. Spectrosc.* 62, 1123–1129. <https://doi.org/10.1016/j.sab.2007.06.015>.
- Fernández-Ruiz, R., Redrejo, M.J., 2018. Effect of modulation of the particle size distributions in the direct solid analysis by total-reflection X-ray fluorescence. *Spectrochim. Acta - Part B At. Spectrosc.* 140, 76–83. <https://doi.org/10.1016/j.sab.2017.12.007>.
- Gerold, G., Lerchhammer, R., Antrekowitsch, H., 2024. Recovery of Cobalt, Nickel, and Lithium from Spent Lithium-Ion Batteries with Gluconic Acid Leaching Process: Kinetics Study. *Batteries* 10. <https://doi.org/10.3390/batteries10040120>.
- Graedel, T.E., Harper, E.M., Nassar, N.T., Reck, B.K., 2015. On the materials basis of modern society. *Proc. Natl. Acad. Sci. USA* 112, 6295–6300. <https://doi.org/10.1073/pnas.1312752110>.
- Greenberg, R.R., Bode, P., De Nadai Fernandes, E.A., 2011. Neutron activation analysis: A primary method of measurement. *Spectrochim. Acta - Part B At. Spectrosc.* 66, 193–241. <https://doi.org/10.1016/j.sab.2010.12.011>.
- Gunn, G. (Ed.), 2014. *Critical Metals Handbook*. John Wiley & Sons Ltd, West Sussex.
- Harouaka, K., Allen, C., Bylaska, E., Cox, R.M., Eiden, G.C., di Vacri, M.L., Hoppe, E.W., Arnquist, I.J., 2021. Gas-phase ion-molecule interactions in a collision reaction cell with triple quadrupole-inductively coupled plasma mass spectrometry: Investigations with N₂O as the reaction gas. *Spectrochim. Acta - Part B At. Spectrosc.* 186, 106309. <https://doi.org/10.1016/j.sab.2021.106309>.
- Horwitz, W., 1982. Evaluation of Analytical Methods Used for Regulation of Foods and Drugs. *Anal. Chem.* 54, 67–76. <https://doi.org/10.1021/ac00238a002>.
- Horwitz, W., Albert, R., 2006. The Horwitz ratio (HorRat): A useful index of method performance with respect to precision. *J. AOAC Int.* 89, 1095–1109. <https://doi.org/10.1093/jaoac/89.4.1095>.
- Hubau, A., Chagnes, A., Minier, M., Touzé, S., Chapron, S., Guezennec, A.G., 2019. Recycling-oriented methodology to sample and characterize the metal composition of waste Printed Circuit Boards. *Waste Manag.* 91, 62–71. <https://doi.org/10.1016/j.wasman.2019.04.041>.

- Hubau, A., Moreau, P., 2022. pXRF on printed circuit boards : Methodology, applications. *And Challenges* 146, 66–76. <https://doi.org/10.1016/j.wasman.2022.05.001>.
- Ippolito, N.M., Belardi, G., Innocenzi, V., Medici, F., Pietrelli, L., Piga, L., 2021. Smart determination of gold content in pcs of waste mobile phones by coupling of xrf and aas techniques. *Processes* 9, 1618. <https://doi.org/10.3390/pr9091618>.
- Jačimović, R., De Corte, F., Kennedy, G., Vermaercke, P., Revay, Z., 2014. The 2012 recommended k0 database. *J. Radioanal. Nucl. Chem.* 300, 589–592. <https://doi.org/10.1007/s10967-014-3085-2>.
- Jenkins, R., 1999. *X-Ray Fluorescence Spectrometry*, 2nd Edit. ed. John Wiley & Sons, Inc., Danvers, MA.
- Klein, O., Zimmermann, T., Pröfrock, D., 2021. Improved determination of technologically critical elements in sediment digests by ICP-MS/MS using N₂O as a reaction gas. *J. Anal. At. Spectrom.* 36, 1524–1532. <https://doi.org/10.1039/d1ja00088h>.
- Klockenkämper, R., Bohlen, A. von, 2014. *Total-Reflection X-Ray Fluorescence Analysis and Related Methods*, 2nd Edit. ed. John Wiley & Sons, Inc. doi: 10.1002/9781118985953.
- Klockenkämper, R., von Bohlen, A., 1989. Determination of the critical thickness and the sensitivity for thin-film analysis by total reflection X-ray fluorescence spectrometry. *Spectrochim Acta - Part B At. Spectrosc.* 44, 461–469. [https://doi.org/10.1016/0584-8547\(89\)80051-5](https://doi.org/10.1016/0584-8547(89)80051-5).
- Lancaster, S.T., Prohaska, T., Irrgeher, J., 2023. Characterisation of gas cell reactions for 70+ elements using N₂O for ICP tandem mass spectrometry measurements. *J. Anal. At. Spectrom.* 38, 1135–1145. <https://doi.org/10.1039/d3ja00025g>.
- Lide, D. (Ed.), 2004. Section 8: Analytical Chemistry, in: *CRC Handbook of Chemistry and Physics*. CRC Press, Boca Raton, FL, pp. 8–110 to 8–118.
- Liu, K., Tan, Q., Yu, J., Wang, M., 2023. A global perspective on e-waste recycling. *Circ. Econ.* 2, 100028. <https://doi.org/10.1016/j.cec.2023.100028>.
- Meisel, T.C., Webb, P.C., Rachetti, A., 2022. Highlights from 25 Years of the GeoPT Programme: What Can be Learnt for the Advancement of Geoanalysis. *Geostand. Geoanalytical Res.* 46, 223–243. <https://doi.org/10.1111/ggr.12424>.
- Ministry of Mines and Energy, 2021. Resolução N°2, de 18 de Junho de 2021.
- Mulcahy, K.R., Kilpatrick, A.F.R., Harper, G.D.J., Walton, A., Abbott, A.P., 2022. Debondable adhesives and their use in recycling. *Green Chem.* 24, 36–61. <https://doi.org/10.1039/d1gc03306a>.
- Qvarforth, A., Lundgren, M., Rodushkin, I., Engström, E., Paulukat, C., Hough, R.L., Moreno-Jiménez, E., Beesley, L., Trakal, L., Augustsson, A., 2022. Future food contaminants: An assessment of the plant uptake of Technology-critical elements versus traditional metal contaminants. *Environ. Int.* 169. <https://doi.org/10.1016/j.envint.2022.107504>.
- R Core Team, 2024. *R: A Language and Environment for Statistical Computing*.
- Stuhlpfarrer, P., Luidold, S., Antrekowitsch, H., 2013. Erhöhung der Verwertungsquoten beim Recycling von Elektronikschrott. *BHM Berg- Und Hüttenmännische Monatshefte* 158, 85–90. <https://doi.org/10.1007/s00501-013-0118-z>.
- Stuhlpfarrer, P., Luidold, S., Antrekowitsch, H., 2016. Recycling of waste printed circuit boards with simultaneous enrichment of special metals by using alkaline melts: A green and strategically advantageous solution. *J. Hazard. Mater.* 307, 17–25. <https://doi.org/10.1016/j.jhazmat.2015.12.007>.
- Thompson, M., 2004. *The amazing Horwitz function*. *AMC Technical Brief No. 17*.
- Touze, S., Guignot, S., Hubau, A., Devau, N., Chapron, S., 2020. Sampling waste printed circuit boards: Achieving the right combination between particle size and sample mass to measure metal content. *Waste Manag.* 118, 380–390. <https://doi.org/10.1016/j.wasman.2020.08.054>.
- Touzé, S., Hubau, A., Ghestem, J.P., Moreau, P., Lafaurie, N., Noireaux, J., 2024. Estimation of the uncertainty of metal content in a batch of waste printed circuit boards from computer motherboards. *Waste Manag.* 189, 325–333. <https://doi.org/10.1016/j.wasman.2024.08.010>.
- Trimmel, S., Meisel, T.C., Lancaster, S.T., Prohaska, T., Irrgeher, J., 2023. Determination of 48 elements in 7 plant CRMs by ICP-MS/MS with a focus on technology-critical elements. *Anal. Bioanal. Chem.* 415, 1159–1172. <https://doi.org/10.1007/s00216-022-04497-3>.
- U.S. Department of Energy, 2023. *Critical Materials Assessment*.
- Umbricht, G., Utters, M., Märki, L., Andres, H., 2022. *Circular economy and metrology*. *OIML Bull.* 63, 5–10.
- Vanhoof, C., Corthouts, V., Tirez, K., 2004. Energy-dispersive X-ray fluorescence systems as analytical tool for assessment of contaminated soils. *J. Environ. Monit.* 6, 344–350. <https://doi.org/10.1039/b312781h>.
- Vanhoof, C., Bacon, J.R., Fittschen, U.E.A., Vincze, L., 2020. 2020 atomic spectrometry update-a review of advances in X-ray fluorescence spectrometry and its special applications. *J. Anal. At. Spectrom.* 35, 1704–1719. <https://doi.org/10.1039/d0ja90051f>.
- Verità, M., Basso, R., Wypyski, M.T., Koestler, R.J., 1994. X-ray microanalysis of ancient glassy materials: A comparative study of wavelength dispersive and energy dispersive techniques. *Archaeometry* 36, 241–251. <https://doi.org/10.1111/j.1475-4754.1994.tb00967.x>.
- Windisch-Kern, S., Gerold, E., Nigl, T., Jandric, A., Altendorfer, M., Rutrecht, B., Scherhauser, S., Raupenstrauch, H., Pomberger, R., Antrekowitsch, H., Part, F., 2022. Recycling chains for lithium-ion batteries: A critical examination of current challenges, opportunities and process dependencies. *Waste Manag.* 138, 125–139. <https://doi.org/10.1016/j.wasman.2021.11.038>.
- Younis, A., Ahmadi, Z., Adams, M.G., Iqbal, A., 2017. A simple method for quantitative analysis of elements by WD-XRF using variable dilution factors in fusion bead technique for geologic specimens. *X-Ray Spectrom.* 46, 69–76. <https://doi.org/10.1002/xrs.2729>.
- Zhu, Y., Ariga, T., Nakano, K., Shikamori, Y., 2021. Trends and advances in inductively coupled plasma tandem quadruple mass spectrometry (ICP-QMS/QMS) with reaction cell. *At. Spectrosc.* 42, 299–309. <https://doi.org/10.46770/AS.2021.710>.